Synoptic Typing of Multiduration, Heavy Precipitation Records in the Northeastern United States: 1895–2017

CAITLIN C. CROSSETT,[a] LESLEY-ANN L. DUPIGNY-GIROUX,[b] KENNETH E. KUNKEL,[c] ALAN K. BETTS,[d] AND ARNE BOMBLIES[e]

[a] *Department of Geoscience, Hobart and William Smith Colleges, Geneva, New York*
[b] *Department of Geography and Geosciences, University of Vermont, Burlington, Vermont*
[c] *North Carolina Institute for Climate Studies, North Carolina State University, Asheville, North Carolina*
[d] *Atmospheric Research, Pittsford, Vermont*
[e] *Department of Civil and Environmental Engineering, University of Vermont, Burlington, Vermont*

(Manuscript received 13 June 2022, in final form 28 April 2023, accepted 8 May 2023)

ABSTRACT: Much of the previous research on total and heavy precipitation trends across the northeastern United States (herein, the Northeast) used daily precipitation totals over relatively short periods of record, which do not capture the full range of climate variability and change. Less well understood are the characteristics of long-term changes and synoptic patterns in longer-duration heavy precipitation events across the Northeast. A multiduration (1, 2, 3, 7, 14, and 30 days), multi-return-interval (2, 5, 10, and 50 years) precipitation dataset was used to diagnose changes in various types of precipitation events across the Northeast from 1895 to 2017. Increasing trends were found in all duration and return-interval event combinations with the rarest, longest duration events increasing at faster rates than more-frequent, shorter-duration ones. Daily 850-hPa geopotential height patterns associated with precipitation events were extracted from rotated principal component analysis and *k*-means clustering analysis, which allowed for the main synoptic types present as well as their structure and evolution to be analyzed. The daily synoptic patterns thus identified were found to be similar across all durations and return intervals and included coastal low (Northeasters, tropical cyclones, and predecessor rain events), deep trough, East Coast trough, zonal, and high pressure patterns.

KEYWORDS: Precipitation; Synoptic-scale processes; Principal components analysis; Trends

1. Introduction

Multiday and consecutive heavy precipitation events have historically led to catastrophic flooding across the northeastern United States (hereinafter, the Northeast). For example, record rainfall on the multiday precipitation event from 3 to 4 November 1927 led to deadly flooding during the Great Vermont Flood of 1927, with estimated damages totaling $30 million in the state of Vermont alone (Kinnison 1929; Dupigny-Giroux 2002). In addition, Hurricanes Connie and Diane, which occurred a week apart in August 1955, resulted in flooding across New England, with Hurricane Diane alone causing $600 million in estimated damage (Dunn et al. 1955).

Previous evaluations of the changes in total and heavy precipitation over time across the Northeast have relied on daily precipitation totals (e.g., Hayhoe et al. 2007; Frei et al. 2015; Guilbert et al. 2015; Marquardt Collow et al. 2016; Huang et al. 2017; Howarth et al. 2019), with less emphasis on the impacts of multiday or consecutive events. In terms of extreme multiday events (e.g., the top 1% of total event precipitation), Agel et al. (2015) report over 90% of events occurring over a 1–3-day duration. Kunkel et al. (1999) found a 22% increase in 7-day, 1-yr return interval events from 1931 to 1996. With a longer time series (1949–2016) for the Northeast, Kunkel et al. (2020) found statistically significant positive trends (ranging from 5% to 20% per decade) in the frequency of occurrence of 30 of the 35 duration–return interval precipitation events examined (events had durations of 1, 2, 5, 10, 20, and 30 days with return intervals of 1, 2, 5, 10, and 20 years). In analyzing 14-day extreme precipitation events observed between 1915 and 2018, Dickinson et al. (2021) reported an increase in the number of events across much of the Northeast.

Daily heavy precipitation events in the Northeast tend to be associated with large-scale patterns such as tropical cyclones (TCs), extratropical cyclones or synoptic systems, mesoscale convective systems, convection, and fronts (Howarth et al. 2019; Huang et al. 2018; Agel et al. 2015; Kunkel et al. 2012; Schumacher and Johnson 2005). These synoptic patterns were primarily derived from the manual interpretation of pressure, temperature, daily weather maps, storm tracks, archived reports, or radar reflectivity characteristics. In contrast, Agel et al. (2018) used an objective clustering method to identify large-scale meteorological patterns associated with non-TC related daily extreme precipitation events in the Northeast from 1979 to 2008. They classified six different patterns including 1) strong ridge of high pressure most frequent in summer (June, July, and August); 2) weaker ridge as a part of a shallow trough–ridge pattern across southern Canada and northern New England active in summer; 3) deep, negatively tilted wintertime trough; 4) deep, negatively tilted summertime trough); 5) deep, transition season (spring and fall) trough located over the Ohio Valley into the southern tier states; and 6) a trough similar to (5) but located farther southwest and occurring in the winter (Agel et al. 2018). While the aforementioned studies only considered daily events, Jennrich et al. (2020)

Corresponding author: Caitlin Crossett, crossett@hws.edu

DOI: 10.1175/JAMC-D-22-0091.1

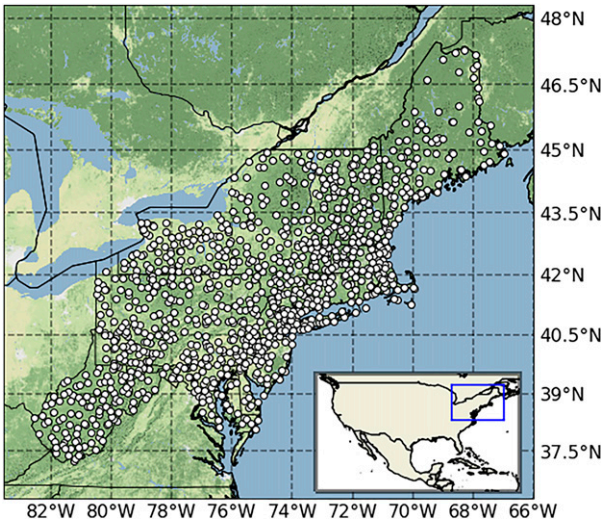

FIG. 1. Spatial extent of the 12 states of the Northeast used in this study. The 1098 National Weather Service COOP stations are shown with white circles.

analyzed composites of 500-hPa standardized height anomalies over 14-day extreme precipitation events from 1981 to 2010 and found a persistent trough–ridge pattern, with a trough to the west of the Northeast and ridge to the east.

Multiple studies have identified trends associated with daily heavy precipitation events in the Northeast (Hayhoe et al. 2007; Frei et al. 2015; Guilbert et al. 2015; Marquardt Collow et al. 2016; Huang et al. 2017; Howarth et al. 2019), and their synoptic types (Henny et al. 2022; Howarth et al. 2019; Huang et al. 2018; Agel et al. 2015; Kunkel et al. 2012; Schumacher and Johnson 2005). This study seeks to extend the aforementioned studies by exploring multiduration, multi-return-interval precipitation events over the Northeast in the 1895–2017 period. In doing so, the interannual variability of these events is quantified, recent increases in precipitation are placed into their historical context and a broader understanding of changes beyond a single statistical threshold, presented. The latter is of critical importance in the realm of engineering design. In addition, this study used an objective synoptic typing methodology to identify the structure of daily synoptic patterns present in the dataset. Presenting trends in multiduration heavy precipitation events alongside their typical synoptic type allows for future analysis of the drivers of the identified increases in precipitation.

2. Data and methods

a. Precipitation dataset

The precipitation dataset was generated from 1098 long-term National Weather Service Cooperative Observer (COOP) stations available from 1895 to 2017 across the Northeast. The spatial extent of the Northeast matches that of the Fourth and Fifth National Climate Assessments, encompassing the states of New York, New Jersey, Pennsylvania, Vermont, New Hampshire, Rhode Island, Massachusetts, Connecticut, Maine, Delaware, Maryland, and West Virginia (Dupigny-Giroux et al. 2018; Fig. 1).

TABLE 1. Percent of days of a specific duration (columns) that are also counted within a longer-duration event (rows) of the same return interval.

Return interval	Duration (N days)	1 day	2 day	3 day	7 day	14 day
50 yr	2 day (830)	40.8	—	—	—	—
	3 day (1147)	27.5	56.8	—	—	—
	7 day (2608)	12.1	21.7	30.8	—	—
	14 day (4315)	6.8	11.4	16.5	41.7	—
	30 day (7609)	4.2	6.7	9.6	23.2	42.9
10 yr	2 day (3227)	50.2	—	—	—	—
	3 day (4353)	35.9	62.6	—	—	—
	7 day (8180)	19.4	30.5	42.4	—	—
	14 day (12 549)	13.3	20.4	27.8	53.4	—
	30 day (18 966)	9.7	14.6	19.7	37.8	58.3
5 yr	2 day (5497)	55.0	—	—	—	—
	3 day (7040)	41.3	67.3	—	—	—
	7 day (12 608)	24.0	36.3	47.0	—	—
	14 day (18 275)	17.6	26.0	33.4	59.6	—
	30 day (25 188)	13.5	19.7	25.3	45.4	66.2
2 yr	2 day (9781)	61.0	—	—	—	—
	3 day (12 351)	48.1	71.4	—	—	—
	7 day (19 911)	31.2	44.0	55.8	—	—
	14 day (27 068)	24.0	33.4	42.2	68.2	—

Stations with at least 10 years of data (which did not have to be continuous in time) available in the 1989–2016 period were included in this study. This criterion allowed for the inclusion of a large number of stations, some with record lengths dating back to the late-1800s from which long-term trends in precipitation could be computed.

b. Event identification, trend, and changepoint analyses

As outlined in Kunkel et al. (1999, 2003) precipitation events with durations of 1, 2, 3, 7, 14, and 30 days, which met thresholds defined by return intervals of 2, 5, 10, and 50 years, were extracted from the COOP network. Precipitation event durations were defined as precipitation accumulation over any N consecutive days (where N were the 1-, 2-, 3-, 7-, 14-, and 30-day durations as defined above) that met or exceeded the return interval thresholds considered. The thresholds for analysis were identified using a partial duration series analysis based on an individual station's climatology. First, the precipitation events were ranked by magnitude, the event of rank one was determined, and the day(s) corresponding to that event were removed from the time series. Then, the second-ranked event was determined by finding the highest-ranking event in the remaining data. This procedure was repeated until N events were identified where $N = M_y/R$, with M_y being the number of years of data and R being the return period in years (Kunkel et al. 2003). This entire process was then repeated for all duration–return interval combinations. Note that, while some days were counted as events for multiple duration–return interval combinations, given the length of the entire period of record and the large number of stations

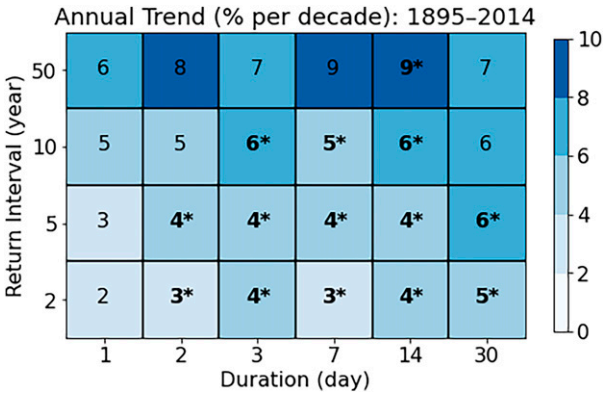

FIG. 2. Annual trends (percent per decade) in the precipitation index (mm per station) for each combination of duration–return intervals in the 1895–2014 period. The magnitude of the decadal increase is shown both numerically and via the color graduation. Numerical values in boldface type with an asterisk represent trends that were significant to 95% confidence as determined by the Mann–Kendall test.

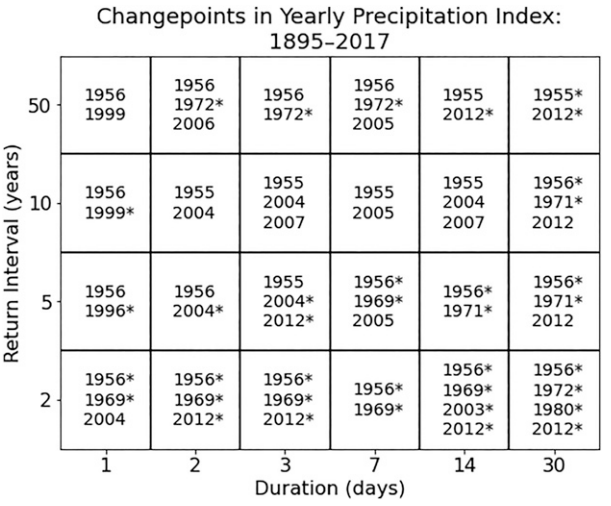

FIG. 3. Changepoints identified in the yearly precipitation index time series from 1895 to 2017 for each duration–return interval combination. Years with an asterisk indicate that the changepoint was statistically significant to 95% confidence using Welch's unequal variances t test ($p < 0.05$).

used in this study, the interpretation of the results was not affected adversely (Table 1 shows the number of N-day events that were captured in different durations of the same return interval). By relying on the thresholds based on the climatology at an individual station, the derived dataset using return intervals to define precipitation events is more robust for use in resilience planning than are the more traditional statistical thresholds such as the 99th percentile, because return intervals of precipitation events are used in engineering design applications. In addition, the dataset allows for the inclusion of more than one heavy precipitation event per year as compared with an annual maximum event selection method.

A yearly precipitation index was calculated to determine the relative magnitude of precipitation that fell every year from each duration–return interval event combination across the Northeast. For each year, the total amount of precipitation that fell above a given threshold in question was accumulated over stations with sufficient data (>300 days yr^{-1}). This yearly value of precipitation was then divided by the number of stations with sufficient data to produce a yearly precipitation index with units of millimeters per station. For example, if a total of 20 mm of precipitation fell above a certain return interval threshold in a year that had 40 stations with sufficient data, that year's precipitation index would be 0.5 mm per station. Scaling the amount of precipitation that fell above a given threshold by the number of stations with sufficient data each year, reduced the impact of stations coming in and out of the record and the increase in the number of stations over time. Decadal trends in the precipitation index were calculated by summing up the yearly index values over a 10-yr period and applying the Mann–Kendall test from the *pymannkendall* module to them in the Python software language (Mann 1945; Kendall 1948; Hussain and Mahmud 2019).

The *findchangepoints* function in Matlab software was used to identify abrupt shifts in the mean of the yearly precipitation index, that is, changepoints, in the dataset (Killick et al. 2012). In the dataset used in this study, an identified changepoint could represent a change from pluvial (increased precipitation) conditions to drier conditions or from drier conditions to pluvial conditions. The *findchangepoints* function in Matlab identifies years that partition the yearly precipitation dataset into two time periods such that the mean of the yearly precipitation before and after that partition changes most significantly. While previous studies have limited the number of changepoints to one (e.g., Huang et al. 2017), this study allowed the maximum number of changepoints to vary from one to eight, given the hypothesis that more than one significant changepoint existed in the long-term precipitation records. Therefore, the *findchangepoints* function may have split the yearly precipitation dataset into more than two segments, depending on the number of changepoints that were retained. An iterative process was used to determine the appropriate number of changepoints to be kept for each duration–return interval combination, with the goals of simultaneously reducing 1) the total residual error of adding additional changepoints (error decreases with each additional changepoint) and 2) the number of changepoints that isolated single-year values in the precipitation index time series. Significance across changepoints was determined using Welch's unequal variances t test ($p < 0.05$). For a set of changepoints that isolated fewer than three years of the time series, the changepoint that resulted in a significant result from Welch's unequal variances t test, or the one with a smaller p value (in the case that neither changepoint resulted in a significant change) was retained.

c. *Synoptic typing analysis*

Rotated principal component analysis (RPCA; Richman 1986) and k-means clustering were used to objectively extract daily synoptic types associated with each duration–return interval combination. RPCA was applied to the daily average

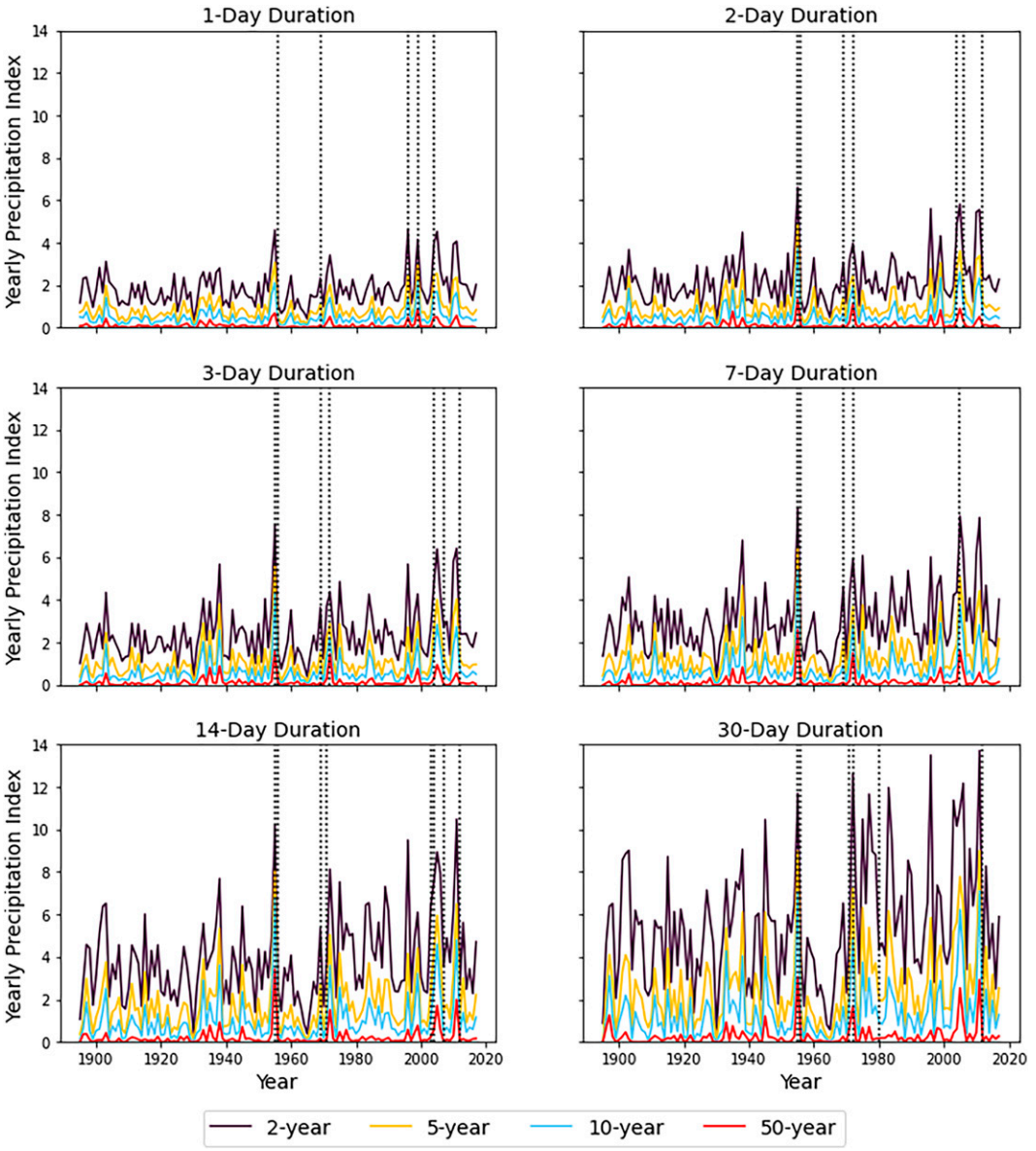

FIG. 4. Yearly precipitation index for each duration–return interval combination overlaid with the changepoints identified in Fig. 3 (black dotted vertical lines). Note that not all changepoints plotted for a given duration (i.e., panel) are representative of all durations. See Fig. 3 for changepoints consistent with each duration–return interval combination.

850-hPa geopotential height data at 936 grid points over the geographic region 25°–50°N and 95–60°W for the period 1895–2015. These upper-level gridded data were extracted from version 3 of the NOAA–CIRES–DOE Twentieth Century Reanalysis (20CRv3) provided by the NOAA/OAR/ESRL PSL (https://psl.noaa.gov/data/gridded/data.20thC_ReanV3.html) (Slivinski et al. 2021; Compo et al. 2011). The 20CRv3 data have a spatial resolution of 1.0° latitude by 1.0° longitude and have been shown to reliably reconstruct weather events and long-term climate trends when compared with other reanalyses and independent observations (Slivinski et al. 2021). The synoptic typing analysis only extends through the year 2015, which was the end of data coverage in the 20CRv3 dataset.

Objective grouping of RPCA loadings using *k*-means clustering was performed following the methodology outlined in Mercer et al. (2012) and Peters and Schumacher (2014). For each set of duration–return interval combinations, the 850-hPa geopotential height patterns associated with all event dates were used and were standardized to remove seasonal impacts. The input matrix of 850-hPa heights was in the T mode (temporal; Richman 1986), given this study's focus on the correlations between individual dates, rather than between grid points (i.e., S mode; Richman 1986). Next, the principal component (PC) loading matrix was calculated using a truncated version of the eigenvector matrix and corresponding eigenvalues. The scree test and the eigenvalue separation test of

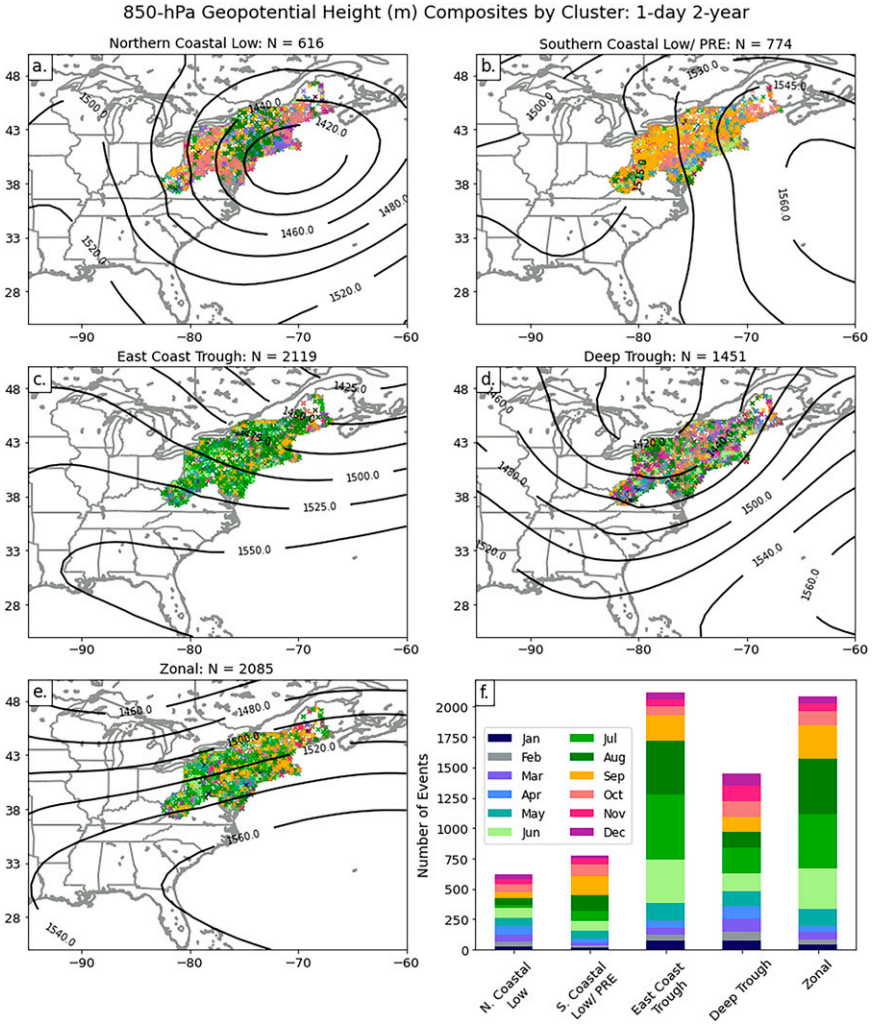

FIG. 5. (a)–(e) Composites of the 850-hPa geopotential height (black contours; m) of the five patterns produced by the *k*-means clustering of the RPCA loading values for 1-day 2-yr events. Crosses indicate the locations of stations, with precipitation events colored by the month of occurrence [as per the key in (f)]. The number of stations with precipitation events (as indicated by the crosses) decreased as the number of days averaged in the composites increased (i.e., longer-duration events) or the magnitude of the return interval increased (i.e., events became rarer). (f) The number of events within each of the five clusters by month. See Fig. A1 in the appendix for results plotted on a geographical domain that has been zoomed in to the Northeast region.

North et al. (1982) were used to determine the number of PCs to be kept, and therefore, the truncation of the eigenvectors and eigenvalues. The first PC typically explains the most variance in a dataset, with the explained variance decreasing monotonically in subsequent PCs. In this dataset, PC1 accounted for 47%–57% of the variance, depending on duration–return interval combination. The first seven PCs for all event combinations were retained, using the tests described above, accounting for 92%–95% of the explained variance. Finally, the truncated PC loading matrix was linearly transformed using the Varimax rotation (Richman 1986), to produce atmospheric patterns that were more realistic and physically interpretable (Richman 1986; Mercer et al. 2012; Peters and Schumacher 2014). Running RPCA on the 850-hPa maps first, ensured that the variability of patterns within groups was captured as compared with using an unsupervised averaging approach that would have likely averaged out the variability in the mean atmospheric state (Mercer et al. 2012).

The *k*-means clustering method (Diday and Simon 1976), from the *sklearn.cluster* module in Python (Pedregosa et al. 2011) was applied to the RPCA loadings on each date, to identify the individual synoptic map types associated with each duration–return interval combination. Performing *k*-means clustering on RPCA loadings reduces the possible impacts of RPCA loadings isolating localized significant features that are not representative of the synoptic pattern (Richman and Mercer 2012;

TABLE 2. Percent of the total number of days associated with the five synoptic types that fell within a given duration–return interval combination.

Return interval	Synoptic type	1 day	2 day	3 day	7 day	14 day	30 day
50 yr	Northern coastal low	16.3	14.3	13.5	10.9	—	—
	Deep trough	19.8	19.5	24.1	19.3	9.3	14.4
	East Coast trough	21.1	25.2	17.4	26.5	24.4	22.7
	High pressure	—	—	—	—	7.5	7.4
	Southern coastal low/PRE	7.8	9.0	10.6	7.3	—	—
	Upstream trough	—	—	—	—	21.7	21.6
	Zonal	35.0	31.9	34.4	36.1	37.1	34.0
10 yr	Northern coastal low	14.2	9.2	8.3	8.3	—	—
	Deep trough	22.1	17.3	18.1	15.7	11.8	17.1
	East Coast trough	19.8	34.6	34.1	34.8	24.7	20.7
	High pressure	—	—	—	—	6.8	7.3
	Southern coastal low/PRE	—	11.3	10.3	9.9	—	—
	Upstream trough	9.9	—	—	—	21.1	22.1
	Zonal	33.9	27.7	29.3	31.4	35.6	32.8
5 yr	Northern coastal low	13.1	9.0	8.6	—	—	—
	Deep trough	22.7	20.3	18.4	13.9	18.1	18.0
	East Coast trough	20.8	31.6	33.2	19.7	22.1	21.7
	High pressure	—	—	—	7.2	6.9	7.2
	Southern coastal low/PRE	8.9	11.1	10.8	—	—	—
	Upstream trough	—	—	—	24.1	20.4	20.8
	Zonal	34.5	27.9	29.2	35.2	32.5	32.4
2 yr	Northern coastal low	8.7	8.4	8.9	—	—	—
	Deep trough	20.6	19.1	19.7	16.5	18.3	—
	East Coast trough	30.1	31.3	32.5	20.4	21.9	—
	High pressure	—	—	—	6.8	7.0	—
	Southern coastal low/PRE	11.0	11.2	10.3	—	—	—
	Upstream trough	—	—	—	22.6	20.5	—
	Zonal	30.0	30.0	28.8	33.9	32.3	—

Mercer et al. 2012). Five clusters were kept for each duration–return interval combination based on results from the silhouette score (Rousseeuw 1987), elbow test, and examination of cluster output. Composites were created for each cluster by averaging the 850-hPa geopotential heights at each grid point over all days within that cluster. RPCA and cluster results for 30-day 2-yr events were neither run nor reported because these events accounted for 84% of the total days in the period of record.

3. Results and discussion

a. *Trends and changepoints*

Results indicated increasing trends in precipitation between 1895 and 2014, across all duration and return-interval event combinations (Fig. 2). Trends were only calculated to 2014 due to the use of decadal time periods. Significant increasing trends were found in 83% of the 2- and 5-yr return interval events (1-day duration events did not have significant trends) with magnitudes that ranged from a 2%–6% increase in precipitation per station per decade. The rarest (i.e., 50-yr return interval), longest duration events increased at faster rates than more-frequent, shorter-duration events, a result consistent with Kunkel et al. (2020). All 14-day duration events exhibited significant increasing trends, consistent with results in Dickinson et al. (2021) across much of the Northeast, performed using the 99th percentile of 14-day accumulations. It should be noted that variations in the magnitudes of the increasing trends across all duration–return interval combinations of heavy precipitation events across the Northeast highlight the potential gaps of a single threshold approach. Using a threshold that underestimates the trends in precipitation over time may result in design standards that do not factor in rare, long-duration precipitation events in the future (Kunkel et al. 2020).

The identified increases in precipitation may either be due in part to increases in atmospheric water vapor or precipitable water as temperatures have increased, or attributed to changes in the intensity, frequency, or types of synoptic systems over time (Kunkel et al. 2020). Annual precipitation in the Northeast is expected to increase by a total of 14 mm month^{-1} by the end of the century (2071–2100) under the highest emission scenario (RCP8.5; Lynch et al. 2016) and if the trends identified in this study continue, much of the future increases in precipitation may fall during the rarest, most impactful events.

The identification of abrupt changes in the time series of the yearly precipitation index can indicate shifts in and the variations of pluvial or dry time periods across the Northeast. Figure 3 lists the years associated with each changepoint identified for all duration–return interval combinations. The time series of the

TABLE 3. Percent of total event days by month within 50-yr return interval events.

Duration–return interval	Synoptic type	Jan	Feb	Mar	Apr	May	Jun	Jul	Aug	Sep	Oct	Nov	Dec
1 day–2 yr	Northern coastal low	4.1	6.2	9.4	12.5	11.0	12.5	4.4	9.3	7.3	10.7	6.7	6.0
	Southern coastal low/PRE	1.8	2.3	3.0	4.3	8.5	10.9	10.2	16.9	20.3	12.8	6.1	3.0
	East Coast trough	3.4	2.4	2.6	2.7	7.0	16.8	25.3	20.9	9.9	3.7	2.5	2.8
	Deep trough	5.2	5.0	7.4	7.2	8.1	10.5	14.6	8.8	8.5	8.8	8.9	7.0
	Zonal	2.2	1.8	3.1	2.3	6.9	15.8	21.6	21.7	13.5	5.4	3.0	2.7
1 day–50 yr	Northern coastal low	0.0	1.1	8.0	8.0	4.5	14.8	5.7	13.6	18.2	14.8	5.7	5.7
	Southern coastal low/PRE	0.0	0.0	0.0	0.0	0.0	14.3	2.4	16.7	35.7	26.2	4.8	0.0
	East Coast trough	2.6	0.9	2.6	3.5	4.4	20.2	21.1	22.8	13.2	7.0	0.9	0.9
	Deep trough	0.9	0.0	4.7	4.7	4.7	9.3	16.8	18.7	17.8	11.2	7.5	3.7
	Zonal	1.1	0.5	0.0	1.6	5.8	13.8	29.1	25.4	16.4	2.6	1.6	2.1
3 day–50 yr	Northern coastal low	1.3	0.6	7.1	11.6	7.1	11.6	7.1	17.4	12.3	11.0	6.5	6.5
	Southern coastal low/PRE	0.0	0.0	0.8	1.6	3.3	7.4	1.6	15.6	27.9	31.1	9.0	1.6
	East Coast trough	2.5	4.0	4.0	2.5	4.0	14.1	19.6	24.1	14.1	6.5	0.0	4.5
	Deep trough	1.8	0.7	2.2	2.2	4.0	13.4	18.1	22.5	20.7	9.1	4.3	1.1
	Zonal	0.8	0.3	3.5	2.5	4.8	11.9	28.9	25.6	15.2	1.3	2.3	3.0
14 day–50 yr	High pressure	0.0	0.0	0.6	0.6	2.8	6.5	8.4	22.0	38.1	17.3	2.5	1.2
	Upstream trough	1.6	1.3	3.5	4.0	8.9	11.0	18.0	21.4	11.0	10.2	4.7	4.4
	East Coast trough	2.4	1.4	3.1	2.6	8.7	13.5	16.6	21.7	11.8	9.3	4.3	4.6
	Deep trough	1.5	1.2	7.2	6.0	12.2	15.6	12.2	12.2	10.2	9.9	6.5	5.5
	Zonal	2.7	1.9	1.8	1.8	6.1	10.2	29.9	24.4	9.7	4.7	3.2	3.6

yearly precipitation index for a given duration (each panel of Fig. 4) and return interval (each line on Fig. 4) are plotted on Fig. 4 and include the location of each changepoint within that time series. Figures 3 and 4 must be used together to identify which changepoints are associated with a time series for the yearly precipitation index for a given duration–return interval combination. A changepoint was observed in 1955 or 1956 for all duration–return interval combinations (Fig. 3). The changepoint identified in 1955 is coincident with an increase in the yearly precipitation index (Fig. 4), possibly related to the aforementioned, record-setting 1955 Atlantic basin hurricane season in which Hurricanes Connie and Diane (the first billion-dollar hurricane) occurred (Dunn et al. 1955). The 1956 changepoint corresponded to a subsequent decrease in the yearly precipitation index (Fig. 4). Significant changepoints were also observed in the late 1960s–early 1970s at several duration–return interval combinations (Fig. 3). These likely represent the shift out of the droughts observed over extended spatial and temporal scales for the Northeast in the early-to-mid-1960s (Namias 1966, 1983), as illustrated by a relative minimum in the yearly precipitation index across all durations and return intervals, to an increase in the yearly precipitation index in the 1970s (Fig. 4). The changepoints in 1955–56 and late-1960s/early 1970s were consistent with shifts in biospheric responses to climate from 1900 to 2012 across the

TABLE 4. Pairing of the PREs associated with Atlantic Basin TCs from 1988 to 2010 and reported in Table 1 of Moore et al. (2013) with the corresponding events in this study. Details on the TC characteristics [year, initiation time (UTC) and date, and geographical region] were determined by Moore et al. (2013). States listed in the geographical area contained one or more stations with a precipitation event that met or exceeded the 1-day *Y*-yr return interval threshold; the asterisk denotes those that had tropical cyclone impacts mentioned in storm event reports extracted from the NOAA/NCEI Storm Events Database. States are listed using U.S. Postal Service abbreviations.

TC (year)	Initiation time (UTC) and date of PRE	Geographical area	Return interval of 1-day events in PRE clusters	States with event on initiation date of PRE
Erin (1995)	1500 UTC 4 Aug	OH/PA/NY	2 yr	NY/VT
Danny (1997)	0500 UTC 24 Jul	NJ/PA	2 yr	NJ*/PA*/NY/MD/WV
Bonnie (1998)	0400 UTC 26 Aug	PA/NY/NY/CT	2, 5 yr	—
Bonnie (1998)	1200 UTC 26 Aug	NY/NJ/CT (off coast)	2, 5 yr	—
Bonnie (1998)	0300 UTC 27 Aug	NY/NJ/CT (off coast)	2, 5 yr	NJ*
Isabel (2003)	0700 UTC 15 Sep	PA/MD/NJ	5 yr	MD*/DE
Frances (2004)	0400 UTC 8 Sep	NY/CT	2, 5, 10, 50 yr	NY*/CT*/PA/WV
Katrina (2005)	0000 UTC 30 Aug	NY/PA/ME	2, 5, 10 yr	NY*/PA*/ME/MA*/RI/WV
Katrina (2005)	0000 UTC 31 Aug	MA/CT/ME	2, 5, 10 yr	ME/NY/PA*/VT

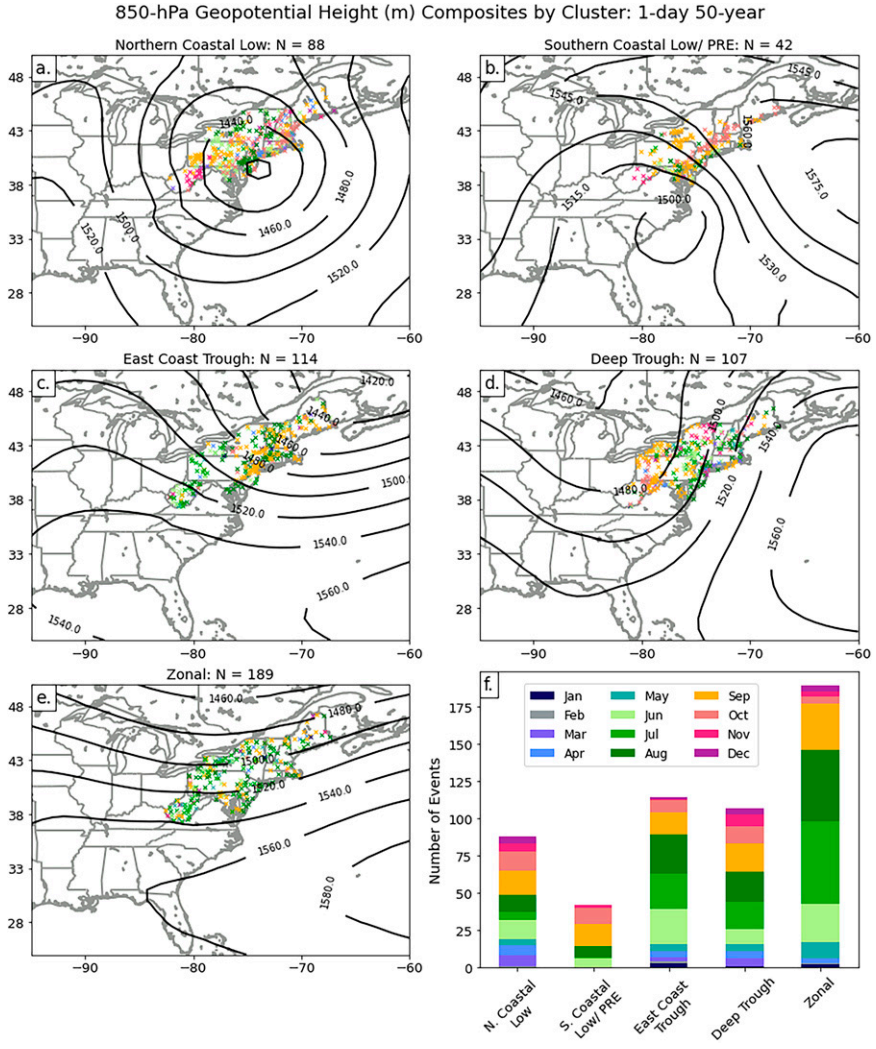

FIG. 6. As in Fig. 5, but for 1-day 50-yr events. See Fig. A2 in the appendix for results plotted on a geographical domain that has been zoomed in to the Northeast region.

Northeast. Using reconstructions of water use efficiency and internal leaf CO_2 concentration derived from networks of tree-ring chronologies from northern hardwood–hemlock forests in the Northeast, Rayback et al. (2020) and Belmecheri et al. (2021) found three distinct periods in those variables from 1900 to 1956, from 1957 to 1975, and from 1976 to 2010 [1901–56 and 1976–2012 in Belmecheri et al. (2021)]. While the 1970s changepoint occurred later in the biospheric reconstructions, this may be due to lagged impacts of the 1960s drought on the trees sampled (Rayback et al. 2020; Belmecheri et al. 2021).

The pluvial period of the post-1970s continued through 2017 with intermittent low yearly precipitation index periods observed in the late 1990s and early-to-mid-2000s, consistent with drought events identified in previous literature (Figs. 3, 4; Seager et al. 2012). The 1996 changepoint found in 1-day 5-yr return interval events was consistent with that found in Huang et al. (2017) for their set of extreme precipitation events (1% of wet days recording the most precipitation from 1901 to 2014) across the Northeast. It is important to note that the changepoints from 1996 to 2012 highlight an increased variability in moisture conditions across the Northeast, with 8 of the 14 changepoints in the 123-yr period of record observed since 1990 alone (Figs. 3, 4). The consistency in the timing of the changepoints in both the observational precipitation record and reconstructed tree-ring chronologies speaks to the robustness of the changepoint identification procedure and underlying land surface process dynamics.

b. *Synoptic typing*

To identify individual synoptic types associated with each duration–return interval combination, *k*-means clustering was applied to the RPCA loadings of all days within a given duration–return interval. Composites were created using all days within each cluster for each duration–return interval combination. For each of the five clusters retained for a given duration–return interval combination, the daily 850-hPa geopotential height

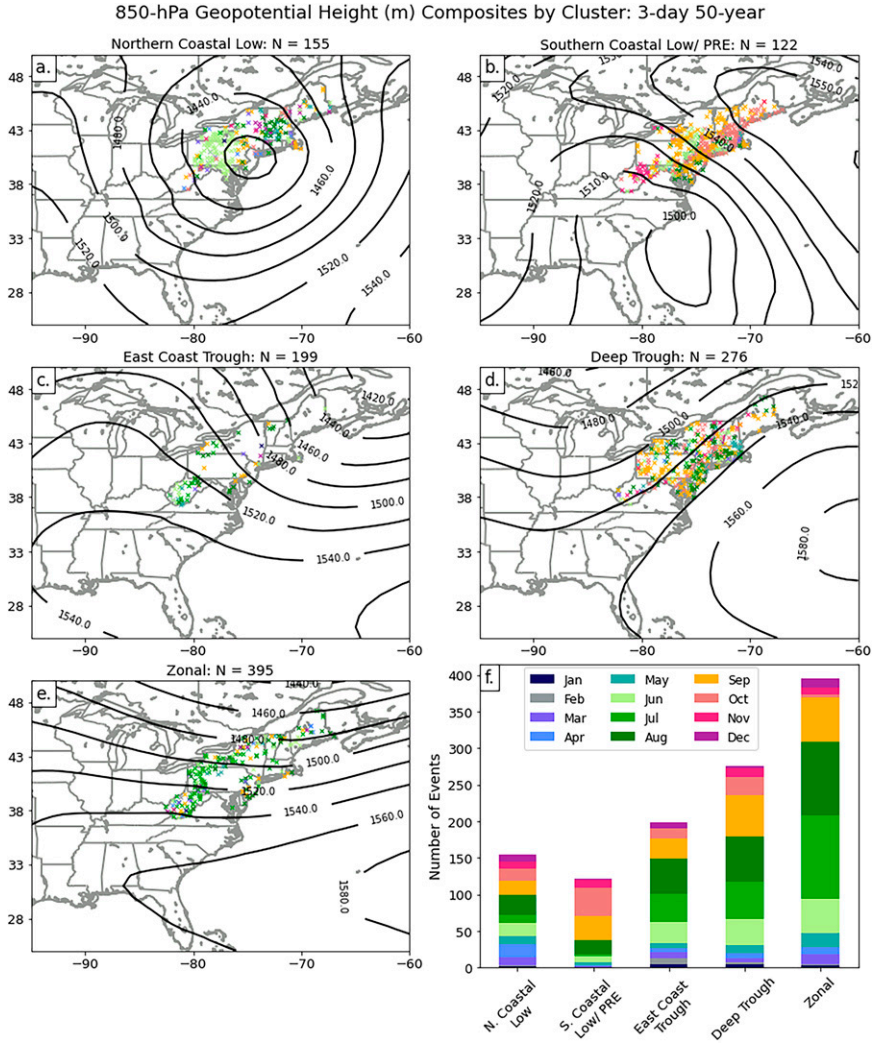

FIG. 7. As in Fig. 5, but for 3-day 50-yr events. See Fig. A3 in the appendix for results plotted on a geographical domain that has been zoomed in to the Northeast region.

patterns associated with the dates within a cluster, were composited to produce the predominant atmospheric patterns. Using the 1-day, 2-yr events as an example, Figs. 5a–e illustrates the predominance of a northern coastal low, southern coastal low/predecessor rain event, East Coast trough, deep trough, and zonal clusters. Similar patterns and seasonality of occurrences (not shown) across all five clusters were observed for the 2-day 2-, 5-, and 10-yr, 3-day 2-, 5-, and 10-yr, and 7-day 10-yr events. The first synoptic pattern, the northern coastal low, represented 8.7% of the total 1-day 2-yr events and was marked by a 1420 m low pressure system centered just east of Cape Cod, Massachusetts (Table 2; Fig. 5a). Figure 5f shows the monthly occurrences of the five clusters. Events in the northern coastal low cluster (which included TCs, Northeasters, and coastal cyclones more generally) occurred all year with the majority being observed in April, May, and June (12.5%, 11.0%, and 12.5% of events within the cluster, respectively) (Fig. 5f; Table 3).

The second synoptic pattern was a negatively tilted trough located upstream of the Northeast with a tongue of high pressure overspreading the Northeast from the east (Fig. 5b). The 850-hPa height patterns of individual events within this cluster often included a closed low located offshore, along the southern Atlantic Coast (which likely has been averaged out of the composite due to the large number of events, that is, southern coastal low in Fig. 5b). This pattern was observed in 11% of all the 1-day 2-yr events (Table 2), with a maximum in August and September (16.9% and 20.3%, respectively) (Fig. 5f; Table 3), the most active time for TC activity in the Atlantic Basin. It is hypothesized that one mechanism for the observed heavy precipitation within this cluster were interactions of tropical moisture (presumably from a cyclone a large distance away) with a preexisting focus for precipitation in the Northeast (e.g., frontal boundary). Event types such as these were first reported by Cote (2007) and were given the name predecessor rain event (PRE). Galarneau et al. (2010) and

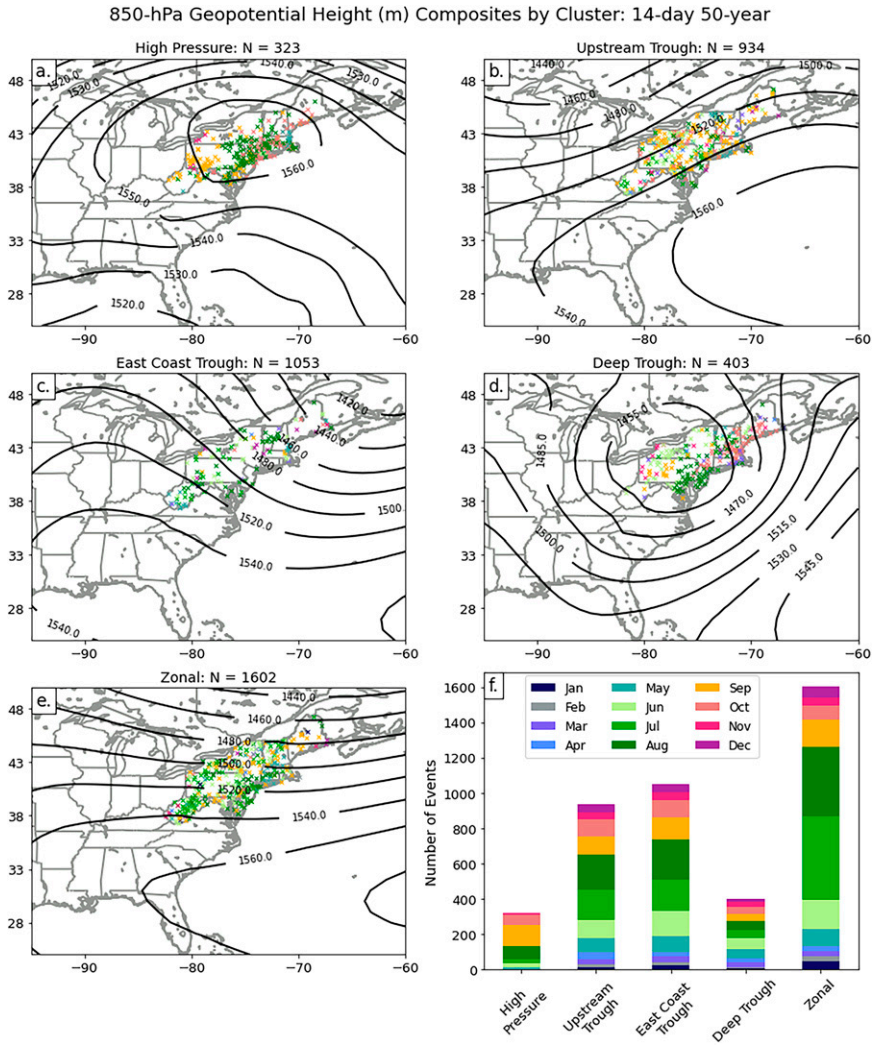

FIG. 8. As in Fig. 5, but for 14-day 50-yr events. See Fig. A4 in the appendix for results plotted on a geographical domain that has been zoomed in to the Northeast region.

Moore et al. (2013) identified PRE events across the United States, including the Northeast, from 1988 to 2010. Their identified events were then compared with the 1-day duration heavy precipitation events found in this study to examine the potential causes of events within the southern coastal low/PRE cluster (Fig. 5f). Storm reports from NOAA's Storm Events Database (https://www.ncdc.noaa.gov/stormevents/) were used to explore the coincidence of TC interactions in relation to the heavy precipitation events identified in this study (Table 4). Six 1-day 2-yr events in this cluster matched previously identified dates of PREs, that impacted any state in the Northeast from 1988 to 2010 reported in Moore et al. (2013; who identified a total of 13 such PREs impacting the Northeast). Events within this cluster that occurred outside of the typical months for TC development may be due to convergence along frontal boundaries or orographic barriers as moist air was transported poleward.

The third synoptic pattern identified was an East Coast trough oriented along the Atlantic coast. It was the most frequently occurring pattern in 1-day 2-yr events (30.1%), with 63% of events within this cluster occurring during the summer months of June, July, and August (16.8%, 25.3%, and 20.9%, respectively; Tables 2, 3; Figs. 5c,f). The fourth synoptic pattern was a deep, neutral-to-positively tilted trough that was associated with 20.6% of 1-day 2-yr events and occurred in all months of the year (Table 2; Figs. 5d,f). Longer durations of this synoptic type exhibited a trough with a positive tilt (not shown). The fifth and final synoptic type (Fig. 5e) was representative of a zonal 850-hPa height pattern across the Northeast with over half of the events in this cluster (59%) occurring in the summer months of June, July, and August (15.8%, 21.6%, and 21.7%, respectively) (Fig. 5f; Table 3). Under weak flow aloft, most events in this cluster were likely convective in nature and consistent with convective precipitation events in previous studies (e.g., Agel et al. 2018; Howarth et al. 2019). Also consistent with previous studies were clusters with extratropical and tropical systems (coastal low clusters; Figs. 5a,b; Howarth et al. 2019; Huang et al. 2018; Agel

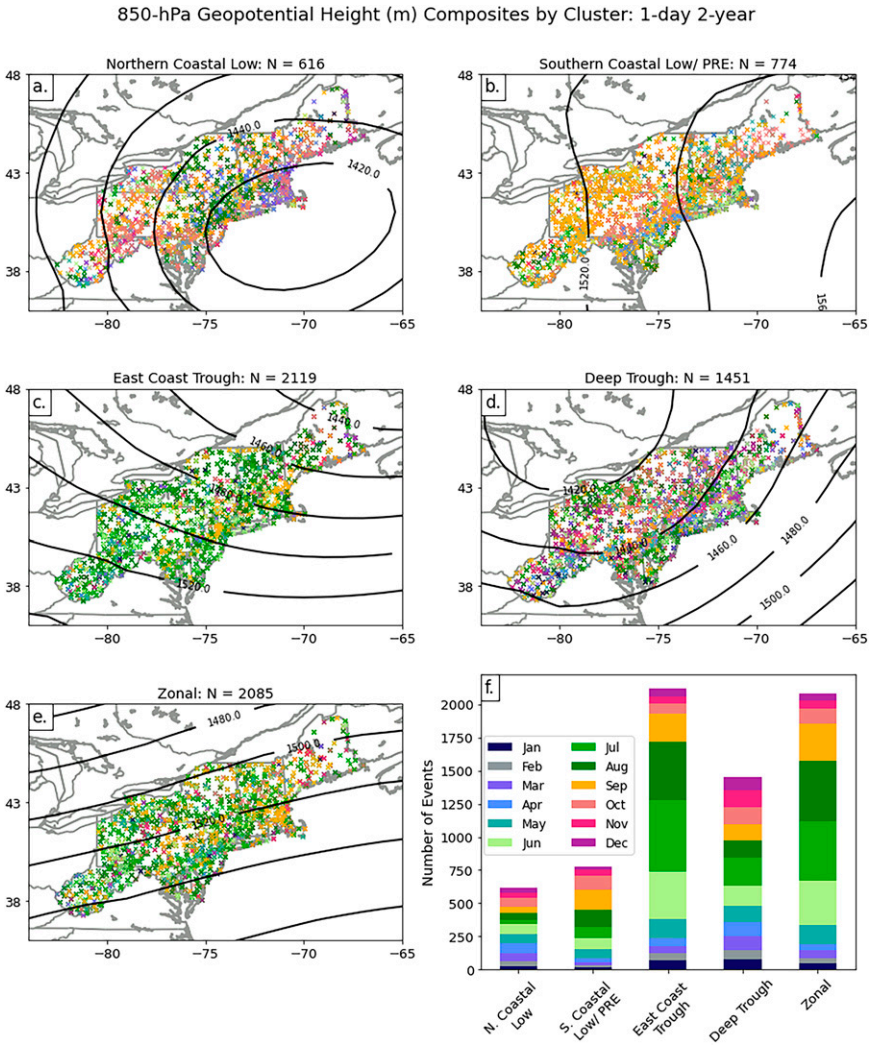

FIG. A1. As in Fig. 5, but for a smaller geographical domain (36°–48°N, 85°–65°W).

et al. 2015; Kunkel et al. 2012; Schumacher and Johnson 2005).

Using the 1-day, 50-yr return interval as an example (Fig. 6), 1-day events with longer return intervals (i.e., 1-day 5-, 10-, and 50-yr events) displayed very similar synoptic patterns and weather events to the 1-day 2-yr events, except for the deep trough cluster. There, the trough axis was negatively tilted (Fig. 6d) as opposed to the neutral or positive tilt in the 1-day 2-yr events (Fig. 5d). This trough was similar to the deep negatively tilted trough identified in Agel et al. (2018; Fig. 6d; their wintertime eastern trough pattern, C2 in their Fig. 4a). The negative tilt of the trough may lead to greater instability over the Northeast, allowing for stronger, deeper systems and the potential for rainfall that meets or exceeds higher return interval thresholds. The southern coastal low/PRE cluster in 1-day 50-yr events occurred in 7.8% of these events and had a more well-defined area of weak low-pressure along the southern Atlantic Coast (as compared with 1-day 2-yr events; Fig. 5b) indicative of a TC (Table 2; Fig. 6b). All events within the southern coastal low/PRE cluster occurred in summer and fall, with maximum occurrences in September and October (35.7% and 26.2%, respectively) (Fig. 6f; Table 3). Many of the stations with heavy precipitation in this cluster were located along the Atlantic coast with fewer stations inland, suggesting direct impacts from TCs and PREs that may have formed ahead of a TC (Fig. 6b). With roughly three-quarters (73%) of events in the northern coastal cluster occurring in summer and fall with a peak in September (18.2%) (Figs. 6a,f; Table 3), many may be due in part to the movement of TCs farther north up the Atlantic Coast, affecting states across the Northeast. It is interesting to note that Agel et al. (2018) found a similar pattern (categorized as the summertime eastern trough pattern, C5 of their Fig. 4a), even though TC related precipitation days were excluded from their analyses.

Although the synoptic types and seasonal distribution of events for 2-, 3-, and 7-day 50-yr events (3-day 50-yr events shown in Fig. 7) were very similar to the aforementioned 1-day events, key differences were noted. These included the

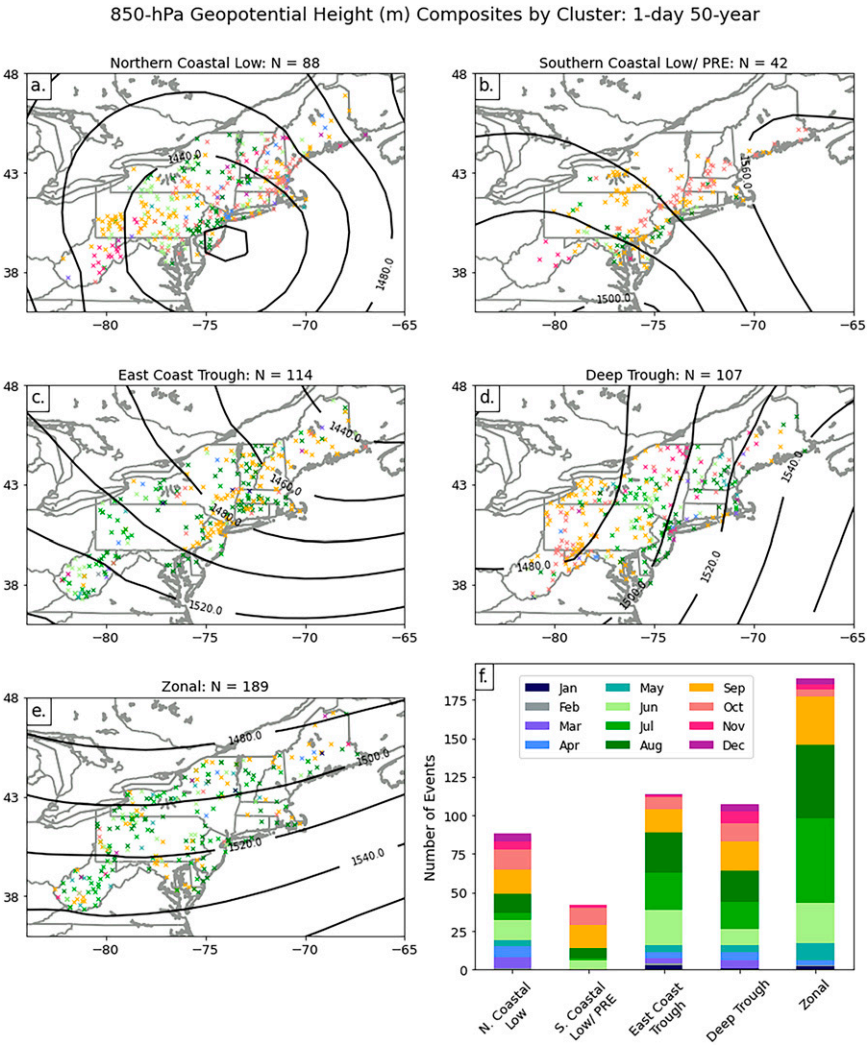

FIG. A2. As in Fig. 6, but for a smaller geographical domain (36°–48°N, 85°–65°W).

location of the trough axis in the deep trough cluster (Fig. 7d) and the location of the center of low pressure in the northern coastal low cluster (Fig. 7a). The deep trough and northern coastal low clusters were associated with a similar portion of the 2-, 3-, and 7-day 50-yr events, with 19.5%, 24.1% and 19.3% of events associated with the deep trough cluster and 14.3%, 13.5%, and 10.9% of events associated with the northern coastal low cluster, respectively (Table 2). In addition, the trough axis in the deep trough cluster was shifted farther west over Lake Michigan, upstream of the Northeast (Fig. 7d), while the center of low pressure in the northern coastal low cluster composite was shifted farther south and west (inland), now centered over New Jersey, in the 2- and 3-day 50-yr events (Fig. 7a; 7-day 50-yr low pressure center is located over the border of western New York and Pennsylvania, not shown). Both the upstream displacement of the trough and the inland migration of the more northern coastal low was likely a reflection of the movement of the trough and coastal low throughout the 3-day duration of the events, since each 850-hPa height pattern, for every day in the 3-day period were included in the RPCA method.

There was a marked shift in the synoptic types at the longer-duration and longer-return-interval events, particularly for the 5-, 10-, and 50-yr return intervals of the 14-day and 30-day durations and the 2- and 5-yr return intervals for the 7- and 14-day durations. A new high pressure cluster was identified and was associated with, on average, 7.1% of the precipitation events within the event types listed above (Table 2). Using the 14-day, 50-yr events as an example (Fig. 8a), the high pressure cluster was observed to occur primarily in August, September, and October (22.0%, 38.1%, and 17.3% of events in the cluster, respectively) (Fig. 8f; Table 3). High pressure days generally preceded precipitation events or marked the transition between precipitation days throughout the 14-day duration of an event, as found by manually analyzing several events (not shown). While the high pressure pattern is not representative of shorter-duration heavy precipitation events it may be reflective of the fact that over longer durations, there

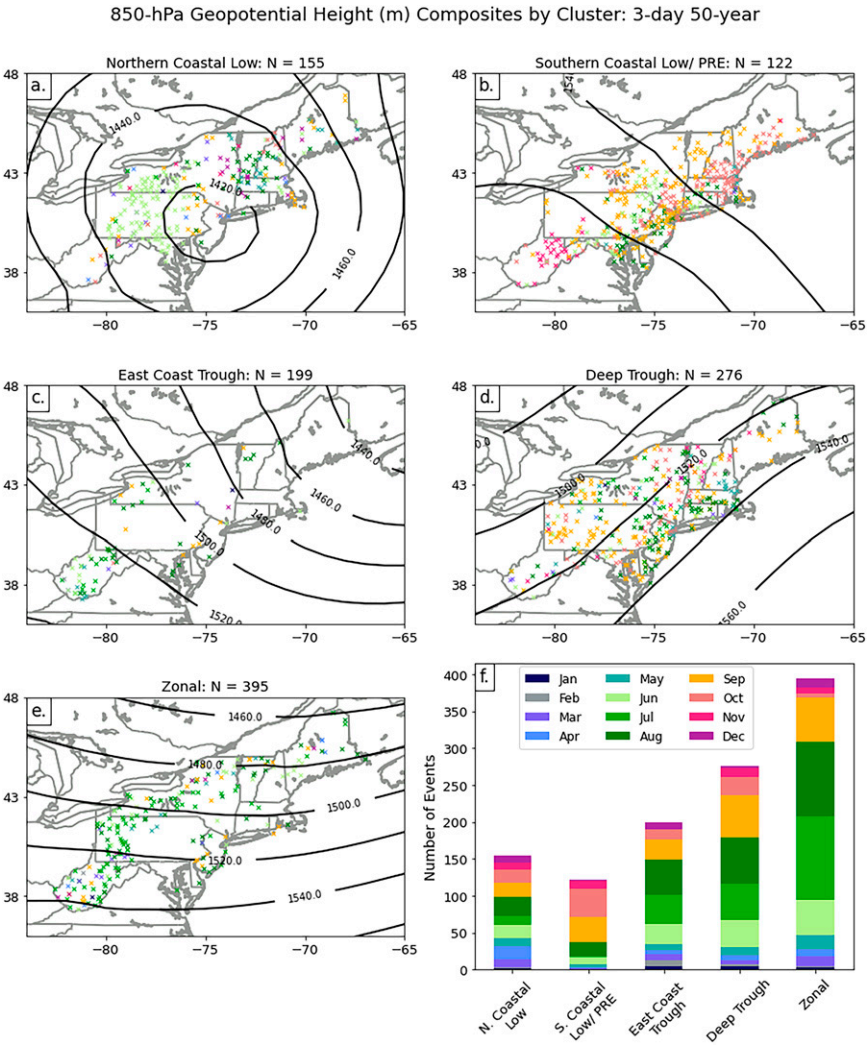

FIG. A3. As in Fig. 7, but for a smaller geographical domain (36°–48°N, 85°–65°W).

are a series of small precipitation events that accumulate to exceed a given return interval threshold. Results from this cluster were consistent with the summertime ridge pattern identified in Agel et al. (2018; C1 of their Fig. 4a). The seasonality and location of features of the deep trough cluster were consistent with 1-day 2-yr events and the East Coast trough cluster were consistent with all other shorter-duration events. The deep trough composite was the only duration–return interval combination with a closed low attendant with the trough; the rest of the events analyzed exhibited an open wave pattern (Figs. 5d, 6d, 7d, 8d). This may indicate that 14-day 50-yr events were associated with more cut-off low patterns, but more information about upper-level characteristics is needed to make this distinction. The upstream trough cluster (Fig. 8b) was consistent with the trough–ridge pattern identified in Jennrich et al. (2020; trough to the west of the Northeast, ridge to the east) and their analysis of synoptic characteristics of 14-day extreme precipitation events.

4. Conclusions

In moving beyond the use of daily precipitation totals to explore heavy precipitation characteristics in the Northeast, this study extends the existing literature via an analysis of multiduration, multi-return-interval precipitation events over the 1895–2017 period of record. Increasing trends in the magnitude of precipitation per station per decade from 1895 to 2014 were found for all duration–return interval combinations analyzed. Our results indicated that the rarest, longest duration events have increased at faster rates than those with shorter durations and return intervals. Fourteen unique changepoints were identified in the yearly precipitation index since 1895. These shifts spanned both the dry-to-wet transitions and vice versa, were spatially coherent and consistent with the timing of similar shifts in climate reconstructions from tree-ring chronologies. Note that the amount of variability between pluvial and dry periods has increased in recent decades, with 8 of the 14 unique changepoints in the 123-yr period of record

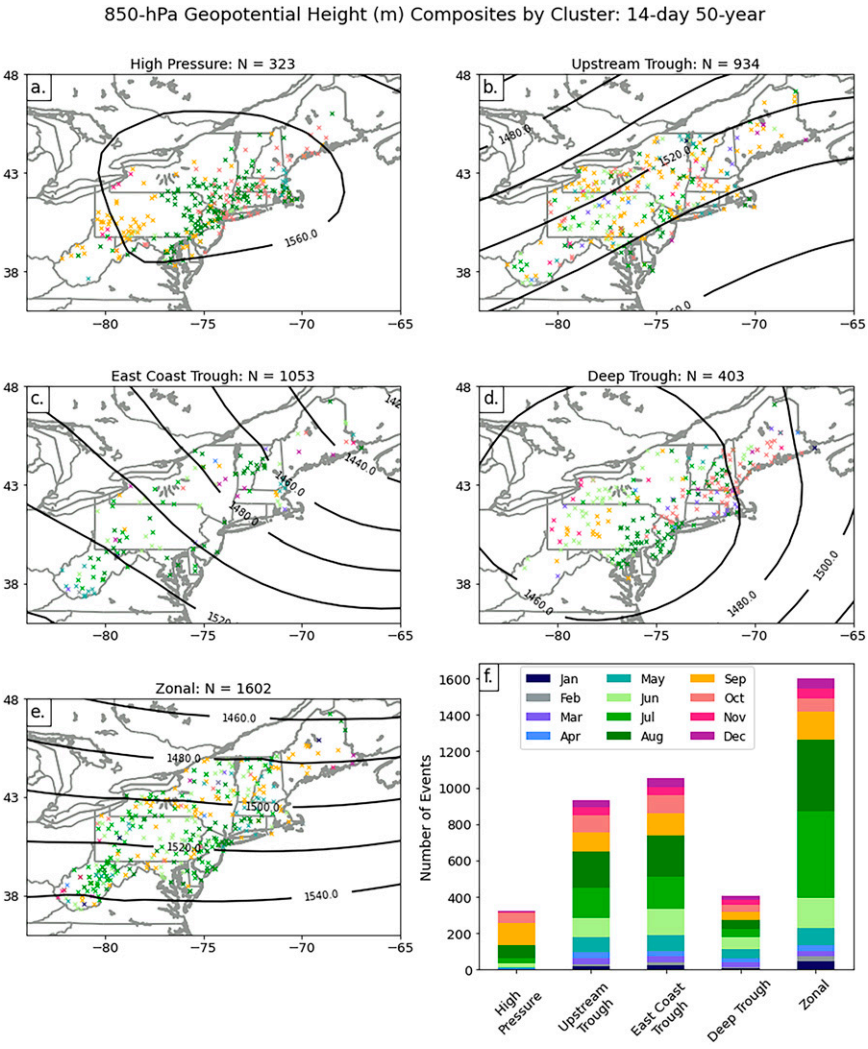

FIG. A4. As in Fig. 8, but for a smaller geographical domain (36°–48°N, 85°–65°W).

being observed since 1996, potentially reflective of the impacts of climate change on precipitation variability in the Northeast. Future work should pursue the underlying causal dynamics for each of the changepoints identified here.

Synoptic-typing results from the *k*-means clustering of RPCA loading values of daily 850-hPa geopotential height patterns for each duration–return interval combination were similar across duration–return interval combinations and times of the year, indicating that many heavy precipitation events across the Northeast were produced by similar types of synoptic systems. The similarities between the short- and long-duration precipitation events may indicate that the longer-duration precipitation events were composed of one or two very heavy short-duration precipitation events and the composites reflected those patterns. These similarities could also mean that the longer-duration events were composed of many small precipitation events, which individually did not exceed the return interval thresholds used in this study, but, when accumulated over the longer duration, were enough to be considered a heavy precipitation event. Future work should include an analysis of the distribution, sequencing, and the magnitude of individual precipitation events within longer-duration events to address the preceding hypotheses. Synoptic patterns included the presence of a coastal low, East Coast trough, upstream trough, PRE, deep trough, zonal, and high pressure. In addition, the synoptic patterns identified in this work were consistent with previous studies that have either objectively classified large-scale patterns associated with daily heavy precipitation events (i.e., Agel et al. 2018) or that consider synoptic patterns associated with longer than one-day duration events (i.e., Jennrich et al. 2020) in the Northeast, although this study considers a wider range of precipitation event durations and magnitudes. This study could be extended with an analysis of the persistence of daily synoptic patterns over longer durations (i.e., 14 and 30 days) in the Northeast. In addition, future analysis of the relative distribution of synoptic types associated with heavy precipitation

events over time could help to uncover the drivers of the identified increases in precipitation as well as further insights on the role of climate change in altering expected precipitation patterns across the Northeast. Once completed, an analysis of the trends in synoptic types over time could be directly compared with the changepoint analysis to identify any changepoints that may relate to changes in trends of synoptic circulations.

Acknowledgments. This material is based upon work supported by the National Science Foundation under Vermont EPSCoR Grant NSF OIA 1556770, the University of Vermont Graduate College, and the NOAA Cooperative Institute for Satellite Earth System Studies under Cooperative Agreement NA19NES4320002. Support for the Twentieth Century Reanalysis Project, version 3, dataset is provided by the U.S. Department of Energy Office of Science Biological and Environmental Research (BER), by the National Oceanic and Atmospheric Administration Climate Program Office, and by the NOAA Physical Sciences Laboratory. We also thank three anonymous reviewers for their valuable contributions to the manuscript version of this paper.

Data availability statement. The data used in this study are freely available online (precipitation data used for event identification, trend, and changepoint analyses: https://www.ncei.noaa.gov/products/land-based-station/cooperative-observer-network; data on the percent of state area in drought or wet conditions: https://www.drought.gov/; 850-hPa geopotential height data used for synoptic typing analyses: https://psl.noaa.gov/data/gridded/data.20thC_ReanV3.html).

APPENDIX

Zoomed-In Figures

Figures A1–A4 are similar to Figs. 5–8, respectively, but have been zoomed into the Northeast domain for clarity.

REFERENCES

Agel, L., M. Barlow, J.-H. Qian, F. Colby, E. Douglas, and T. Eichler, 2015: Climatology of daily precipitation and extreme precipitation events in the northeast United States. *J. Hydrometeor.*, **16**, 2537–2557, https://doi.org/10.1175/JHM-D-14-0147.1.

——, ——, S. B. Feldstein, and W. J. Gutowski, 2018: Identification of large-scale meteorological patterns associated with extreme precipitation in the US northeast. *Climate Dyn.*, **50**, 1819–1839, https://doi.org/10.1007/s00382-017-3724-8.

Belmecheri, S., R. S. Maxwell, A. H. Taylor, K. J. Davis, R. Guerrieri, D. J. P. Moore, and S. A. Rayback, 2021: Precipitation alters the CO_2 effect on water-use efficiency of temperate forests. *Global Change Biol.*, **27**, 1560–1571, https://doi.org/10.1111/gcb.15491.

Compo, G. P., and Coauthors, 2011: The Twentieth Century Reanalysis Project. *Quart. J. Roy. Meteor. Soc.*, **137** (654), 1–28, https://doi.org/10.1002/qj.776.

Cote, M. R., 2007: *Predecessor Rain Events in Advance of Tropical Cyclones*. University at Albany, State University of New York, 200 pp.

Dickinson, T. A., M. B. Richman, and J. C. Furtado, 2021: Subseasonal-to-seasonal extreme precipitation events in the contiguous United States: Generation of a database and climatology. *J. Climate*, **34**, 7571–7586, https://doi.org/10.1175/JCLI-D-20-0580.1.

Diday, E., and J. C. Simon, 1976: Clustering analysis. *Digital Pattern Recognition*, Springer Berlin Heidelberg, 47–94.

Dunn, G. E., W. R. Davis, and P. L. Moore, 1955: Hurricanes of 1955. *Mon. Wea. Rev.*, **83**, 315–326, https://doi.org/10.1175/1520-0493(1955)083<0315:HO>2.0.CO;2.

Dupigny-Giroux, L. A., 2002: Climate variability and socioeconomic consequences of Vermont's natural hazards: A historical perspective. *Vt. Hist.*, **70**, 19–39.

——, and Coauthors, 2018: Northeast. *Impacts, Risks, and Adaptation in the United States: Fourth National Climate Assessment*, Vol. II, U.S. Global Change Research Program, 669–742.

Frei, A., K. E. Kunkel, and A. Matonse, 2015: The seasonal nature of extreme hydrological events in the northeastern United States. *J. Hydrometeor.*, **16**, 2065–2085, https://doi.org/10.1175/JHM-D-14-0237.1.

Galarneau, T. J., L. F. Bosart, and R. S. Schumacher, 2010: Predecessor rain events ahead of tropical cyclones. *Mon. Wea. Rev.*, **138**, 3272–3297, https://doi.org/10.1175/2010MWR3243.1.

Guilbert, J., A. K. Betts, D. M. Rizzo, B. Beckage, and A. Bomblies, 2015: Characterization of increased persistence and intensity of precipitation in the northeastern United States. *Geophys. Res. Lett.*, **42**, 1888–1893, https://doi.org/10.1002/2015GL063124.

Hayhoe, K., and Coauthors, 2007: Past and future changes in climate and hydrological indicators in the US Northeast. *Climate Dyn.*, **28**, 381–407, https://doi.org/10.1007/s00382-006-0187-8.

Henny, L., C. D. Thorncroft, and L. F. Bosart, 2022: Changes in large-scale fall extreme precipitation in the mid-Atlantic and northeast United States, 1979–2019. *J. Climate*, **35**, 3047–3070, https://doi.org/10.1175/JCLI-D-21-0953.1.

Howarth, M. E., C. D. Thorncroft, and L. F. Bosart, 2019: Changes in extreme precipitation in the northeast United States: 1979–2014. *J. Hydrometeor.*, **20**, 673–689, https://doi.org/10.1175/JHM-D-18-0155.1.

Huang, H., J. M. Winter, E. C. Osterberg, R. M. Horton, and B. Beckage, 2017: Total and extreme precipitation changes over the northeastern United States. *J. Hydrometeor.*, **18**, 1783–1798, https://doi.org/10.1175/JHM-D-16-0195.1.

——, ——, and ——, 2018: Mechanisms of abrupt extreme precipitation change over the northeastern United States. *J. Geophys. Res. Atmos.*, **123**, 7179–7192, https://doi.org/10.1029/2017JD028136.

Hussain, M. M., and I. Mahmud, 2019: pyMannKendall: A python package for non parametric Mann Kendall family of trend tests. *J. Open Source Software*, **4**, 1556, https://doi.org/10.21105/joss.01556.

Jennrich, G. C., J. C. Furtado, J. B. Basara, and E. R. Martin, 2020: Synoptic characteristics of 14-day extreme precipitation events across the United States. *J. Climate*, **33**, 6423–6440, https://doi.org/10.1175/JCLI-D-19-0563.1.

Kendall, M. G., 1948: *Rank Correlation Methods*. Charles Griffin & Co., 160 pp.

Killick, R., P. Fearnhead, and I. A. Eckley, 2012: Optimal detection of changepoints with a linear computational cost. *J. Amer. Stat. Assoc.*, **107**, 1590–1598, https://doi.org/10.1080/01621459.2012.737745.

Kinnison, H. B., 1929: The New England flood of November, 1927. *Contributions to Hydrology of United States*, Government Printing Office, 45–100.

Kunkel, K. E., K. Andsager, and D. R. Easterling, 1999: Long-term trends in extreme precipitation events over the conterminous United States and Canada. *J. Climate*, **12**, 2515–2527, https://doi.org/10.1175/1520-0442(1999)012<2515:LTTIEP>2.0.CO;2.

——, D. R. Easterling, K. Redmond, and K. Hubbard, 2003: Temporal variations of extreme precipitation events in the United States: 1895–2000. *Geophys. Res. Lett.*, **30**, 1990, https://doi.org/10.1029/2003GL018052.

——, ——, D. A. R. Kristovich, B. Gleason, L. Stoecker, and R. Smith, 2012: Meteorological causes of the secular variations in observed extreme precipitation events for the conterminous United States. *J. Hydrometeor.*, **13**, 1131–1141, https://doi.org/10.1175/JHM-D-11-0108.1.

——, T. R. Karl, M. F. Squires, X. Yin, S. T. Stegall, and D. R. Easterling, 2020: Precipitation extremes: Trends and relationships with average precipitation and precipitable water in the contiguous United States. *J. Appl. Meteor. Climatol.*, **59**, 125–142, https://doi.org/10.1175/JAMC-D-19-0185.1.

Lynch, C., A. Seth, and J. Thibeault, 2016: Recent and projected annual cycles of temperature and precipitation in the northeast United States from CMIP5. *J. Climate*, **29**, 347–365, https://doi.org/10.1175/JCLI-D-14-00781.1.

Mann, H. B., 1945: Nonparametric tests against trend. *Econometrica*, **13**, 245–259, https://doi.org/10.2307/1907187.

Marquardt Collow, A. B., M. G. Bosilovich, and R. D. Koster, 2016: Large-scale influences on summertime extreme precipitation in the northeastern United States. *J. Hydrometeor.*, **17**, 3045–3061, https://doi.org/10.1175/JHM-D-16-0091.1.

Mercer, A. E., C. M. Shafer, C. A. Doswell, L. M. Leslie, and M. B. Richman, 2012: Synoptic composites of tornadic and nontornadic outbreaks. *Mon. Wea. Rev.*, **140**, 2590–2608, https://doi.org/10.1175/MWR-D-12-00029.1.

Moore, B. J., L. F. Bosart, D. Keyser, and M. L. Jurewicz, 2013: Synoptic-scale environments of predecessor rain events occurring east of the Rocky Mountains in association with Atlantic basin tropical cyclones. *Mon. Wea. Rev.*, **141**, 1022–1047, https://doi.org/10.1175/MWR-D-12-00178.1.

Namias, J., 1966: Nature and possible causes of the northeastern United States drought during 1962–65. *Mon. Wea. Rev.*, **94**, 543–554, https://doi.org/10.1175/1520-0493(1966)094<0543:NAPCOT>2.3.CO;2.

——, 1983: Some causes of United States drought. *J. Climate Appl. Meteor.*, **22**, 30–39, https://doi.org/10.1175/1520-0450(1983)022<0030:SCOUSD>2.0.CO;2.

North, G. R., T. L. Bell, R. F. Cahalan, and F. J. Moeng, 1982: Sampling errors in the estimation of empirical orthogonal functions. *Mon. Wea. Rev.*, **110**, 699–706, https://doi.org/10.1175/1520-0493(1982)110<0699:SEITEO>2.0.CO;2.

Pedregosa, F., and Coauthors, 2011: Scikit-learn: Machine learning in python. *J. Mach. Learn. Res.*, **12**, 2825–2830.

Peters, J. M., and R. S. Schumacher, 2014: Objective categorization of heavy-rain-producing MCS synoptic types by rotated principal component analysis. *Mon. Wea. Rev.*, **142**, 1716–1737, https://doi.org/10.1175/MWR-D-13-00295.1.

Rayback, S. A., S. Belmecheri, M. H. Gagen, A. Lini, R. Gregory, and C. Jenkins, 2020: North American temperate conifer (*Tsuga canadensis*) reveals a complex physiological response to climatic and anthropogenic stressors. *New Phytol.*, **228**, 1781–1795, https://doi.org/10.1111/nph.16811.

Richman, M. B., 1986: Review article: Rotation of principal components. *J. Climatol.*, **6**, 293–335, https://doi.org/10.1002/joc.3370060305.

——, and A. E. Mercer, 2012: Identification of intraseasonal modes of variability using rotated principal components. *Atmospheric Model Applications*, I. Yucel, Ed., Intech, 273–296.

Rousseeuw, P. J., 1987: Silhouettes: A graphical aid to the interpretation and validation of cluster analysis. *J. Comput. Appl. Math.*, **20**, 53–65, https://doi.org/10.1016/0377-0427(87)90125-7.

Schumacher, R. S., and R. H. Johnson, 2005: Organization and environmental properties of extreme-rain-producing mesoscale convective systems. *Mon. Wea. Rev.*, **133**, 961–976, https://doi.org/10.1175/MWR2899.1.

Seager, R., N. Pederson, Y. Kushnir, J. Nakamura, and S. Jurburg, 2012: The 1960s drought and the subsequent shift to a wetter climate in the Catskill Mountains region of the New York City watershed. *J. Climate*, **25**, 6721–6742, https://doi.org/10.1175/JCLI-D-11-00518.1.

Slivinski, L. C., and Coauthors, 2021: An evaluation of the performance of the Twentieth Century Reanalysis version 3. *J. Climate*, **34**, 1417–1438, https://doi.org/10.1175/JCLI-D-20-0505.1.